ADVANCED MATERIALS INTERFACES
www.advmatinterfaces.de

Concentration-Driven Disruption of Single-File Water

*Maria Rezvova, Armin Gölzhäuser, and Petr Dementyev**

Strong hydrogen bonding is known to entail some of the spectacular physical properties of liquid water, including fast diffusion under nanoconfinement. Similar to biological channels, the single-file or collective motion of interconnected water molecules has been observed in nanotubes and laminar structures, exhibiting tremendous potential for energy-efficient separation applications. Desalination, breaking azeotropes, and dehumidification have been all addressed with the membranes enabling selective transport of water while most attention has been paid to the fabrication and morphological characteristics of the respective microporous materials. However, the performance of membrane processes also depends on the properties of the chemical systems to be treated, often facing problems under realistic conditions such as concentration polarization. In this study, adsorption controlled permeation is employed to explore the interfacial behavior of water–alcohol mixtures in nanostructured membranes as a function of concentration. The permeation rate of water is found to sink manifold as the molar fraction of isopropanol molecules increases, indicating breakdown of the single-file mechanism. A phenomenological model is devised to account for intermolecular interactions in the binary liquid–liquid mixture whereas kinetic simulations agree well with the experimental data. The results point to the fundamental limitations of water-selective conduits for dehydrating organic solvents.

1. Introduction

Microporous materials appear to play one of the key roles in the emerging clean-energy technologies.[1] Due to their well-defined pore architectures, zeolites, metal–organic frameworks (MOFs), nanocarbons, etc., reveal a promisingly high efficiency for membrane processes, such as water desalination, fuel cells, and energy storage.[2–5] Graphene oxide (GO) is particularly interesting as this abundant nanostructured material has been widely pursued for diverse practical applications.[6,7] Back in 2012, Nair et al. discovered fast and selective permeation of water in GO membranes which was attributed to the collective flow of hydrogen-bonded molecules through nanochannels between graphene layers.[8] Condensed water was speculated to behave in the 2D capillaries as a single file similar to that in carbon nanotubes and aquaporins.[9] The interlayer spacing in GO laminates was found to shrink upon thermal annealing, and water transport rate was correlated with the number of oxygen-containing functional groups.[10] GO nanochannels were demonstrated to enable filtration of ionic solutes revealing a clear size cutoff at 4.5 Å.[11] In order to allow for controlled ionic sieving, the pore size in GO membranes was later shown to be adjusted by both physical and chemical methods.[12] More recently, water-selective GO membranes were employed in pervaporation to dehydrate ethanol, and the transmembrane flux was measured to depend on the alcohol fraction dropping from 1.36 kg m^{-2} h^{-1} for pure water to 0.3 kg m^{-2} h^{-1} for feed mixtures of 10 wt% water in content.[13] Even though great values of water/ethanol selectivity were achieved, the reduction of the membrane permeability observed indicates complex interfacial phenomena which are likely to differ from those in salt rejection. While the concentration of solid substances in aqueous solutions is limited by saturation points, the composition of liquid mixtures can be varied continuously.

Water is fully miscible with a wide range of polar organic solvents, and membrane separation is considered to be advantageous in their recovery and purification.[14] Unlike ordinary fractional distillation, vapor permeation and pervaporation processes can break azeotropes which is also very important in the biofuel production.[15] Dehydration of organics is the most demanded pervaporation technology in industry, and design of thermally stable membrane materials remains a subject of immense scientific efforts.[16] Porous structures capable of the single-file water transport offer the opportunity to fabricate high-throughput membranes for removing water from liquids. However, the production of anhydrous compounds means selective extraction of water down to ppm levels of the residue, whereas the mass transfer under these circumstances is not necessarily the same as for aqueous solutions, exemplified above by GO membranes. Indeed, bulk properties in the binary water–ethanol mixtures are known to change with the molar composition,

M. Rezvova, Prof. A. Gölzhäuser, Dr. P. Dementyev
Physics of Supramolecular Systems and Surfaces
Faculty of Physics
Bielefeld University
Bielefeld 33615, Germany
E-mail: dementyev@physik.uni-bielefeld.de
M. Rezvova
Research Institute for Complex Issues of Cardiovascular Diseases
Kemerovo 650002, Russian Federation
The ORCID identification number(s) for the author(s) of this article can be found under https://doi.org/10.1002/admi.202000121.

DOI: 10.1002/admi.202000121

and the structure of hydrogen bonding networks has been predicted to differ at higher alcohol concentrations.[17] As revealed by molecular dynamics simulations, 3D water transforms into a nonpercolating phase giving rise to alteration of the dynamical behavior. In this work, we address fundamental issues underlying water permeation in microporous membranes upon mixing with organic solvents. To this end, adsorption controlled permeation (ACP) is applied to study experimentally the impact of concentration on water transport in prototypic carbon nanomembranes (CNMs) with a high density of sub-nanometer channels. Vaporous mixtures of heavy water and isopropanol are introduced as a representative model system allowing to measure the permeation rate in dependence on the molar fraction. The kinetic data obtained with hydrophilic CNMs are rationalized in terms of the single-file mechanism and confirm the disruption of hydrogen bonding networks.

2. Results and Discussion

2.1. Adsorption-Controlled Permeation

The novel ACP methodology has emerged as a versatile tool to probe molecular diffusion at functional interfaces.[18,19] It consists in measuring permeation rates across planar nanomaterials equipped with angstrom-scale openings under well-defined feed environments. Due to the small internal volume, the transmembrane passage is governed by entrance kinetics and depends much on the amount of adsorbed species which imparts high sensitivity to surface processes. **Figure 1**a schematically illustrates the principle of the ACP measurements, while the complete experimental system is detailed elsewhere.[20] A nanomembrane is positioned in a freestanding state between a high-vacuum mass-spectrometric detector and the upstream compartment that is suitable for preparing gaseous and vaporous mixtures of variable composition. Under isothermal conditions, the coverage of adsorbates is determined by equilibrium constants, so that steady-state transport rates are obtained in the ACP experiments. As a rule, the composition of the condensed phase upon mixing several substances deviates from that in the gas phase and obeys thermodynamic relationships. Since vapor–liquid equilibria (VLE) diagrams are usually very complex for nonideal systems, the most favorable situation is reached at azeotropic points, when the mixture composition is maintained constant throughout the feed compartment.

In order to make a vaporous mixture of desirable content, vapor A is let to the mixing chamber and then isolated in the coldfinger by means of a liquid nitrogen bath (Figure 1a). This is done at low relative pressure to exclude vapor condensation on the chamber walls, and the exact amount of the substance is measured with the manometer. Similarly, a portion of vapor B is subsequently dosed to the mixing chamber and collected in the coldfinger. The percentage of each component as well as their total quantity are defined precisely in a broad range. The coldfinger is designed to facilitate intermixing by elevating the temperature, and after cooling down, the freshly prepared feed mixture is released to the nanomembrane. The volume ratio between the sections allows for achieving VLE conditions, when the liquid mixture in the coldfinger yields saturated vapor phase in the entire upstream compartment. Figure 1b demonstrates the evaporation process as recorded by the absolute pressure in the feed chamber and a simultaneous readout of the mass-spectrometer signal in the detection chamber. As evidenced, the total pressure in the system stabilizes rather quickly meaning the homogeneity of the mixture. One can also see that the number of permeating molecules is somewhat delayed from the pressure signal which reflects equilibration of molecular adsorption at the membrane surface. Once the steady state is established, the feed compartment is evacuated leading to the abrupt drop of the mass-spectrometric response. The cross-membrane flux is quantified upon measuring individual calibration signals for the mixture components as described before.[20]

2.2. Room-Temperature Azeotropes

Recently, we presented a convenient model system for studying membrane performance in breaking aqueous azeotropes.[19] The mixture of 60 mol% D_2O and 40 mol% 1-propanol (PA) was proven to be a positive azeotrope at room temperature, as

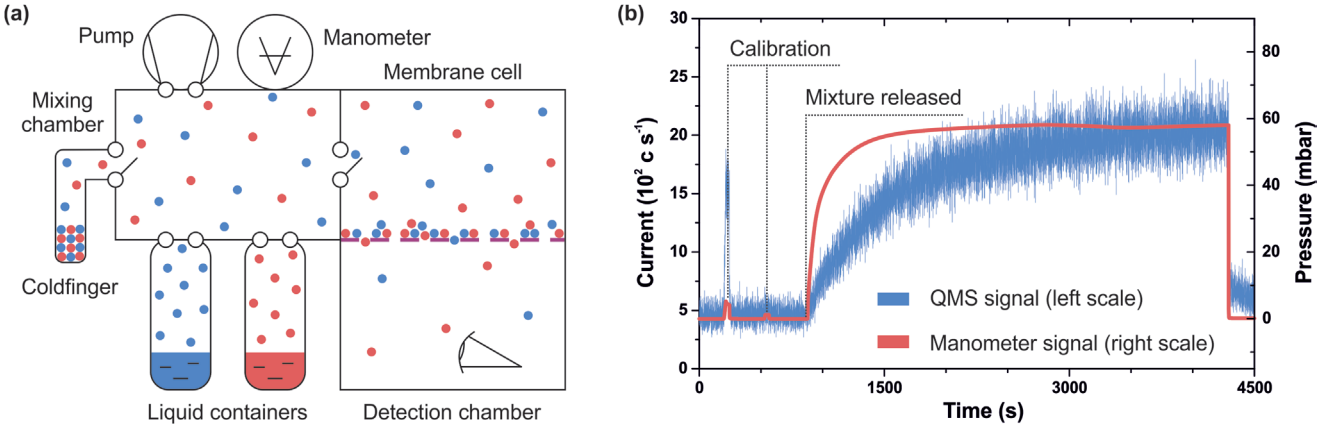

Figure 1. a) Schematic of the ACP measurements with vaporous mixtures. The nanomembrane window is not explicitly denoted as it separates the membrane cell and the detection chamber. b) Example of the raw experimental data for a binary feed mixture. The QMS output for one component (water) is aligned with the total pressure measurement. The QMS signal for the other component (isopropanol) is not shown for simplicity.

expected from H_2O-PA VLE.[21] Upon exposing to the feed mixture, CNMs were found to pass water molecules as fast as water vapor alone indicating unimpeded single-file flow. Previously, freestanding CNMs were proven to possess an intrinsically porous structure enabling collective permeation of liquefied water.[22] In this work, CNMs are used to study the effect of concentration on water transport with the help of another room-temperature azeotrope. VLE data for water mixtures with isopropanol (IPA) suggest the azeotropic point to be shifted toward less diluted alcohol solutions compared to the PA–water system.[23] Similar to the early study, we employed heavy water for accuracy reasons and prepared the mixture of 32 mol% D_2O and 68 mol% IPA. When CNMs are fed with the vapor of this composition, the flux of water decreases greatly with respect to pure D_2O and the PA–water azeotrope (**Figure 2**). Notably, the observed effect cannot be attributed to the decrease in the driving force as the partial pressure of water in the mixture is about 17 mbar, i.e., only 30% lower than saturation pressure of D_2O. The data rather display that more alcohol in the mixture suppresses transmembrane diffusion of water molecules which confirms the theoretical predictions of the concentration-related structural reorganization. Indeed, the isomeric PA and IPA molecules are likely to be identical from the chemical viewpoint, whereas the increase of their molar fraction from 40% to 68% means a dramatic shift in the ratio between water and alcohol in the mixtures. The change from 3:2 in the PA azeotrope to roughly 1:2 in the IPA system points to a fundamental difference in the predominant species: "a solution of alcohol in water" versus "a solution of water in alcohol."

In our understanding, this seemingly fictitious transformation affects the structure of hydrogen bonding networks so as water molecules become less capable of collective motion. This is consistent with the study of Li et al. who employed terahertz time domain spectroscopy and nuclear magnetic resonance measurements to explore structural transitions in binary water–alcohol systems.[24] They found a critical concentration above which the solution dynamics of water and alcohol molecules becomes independent from each other suggesting water clusters in bulk alcohol. It is 70 mol% for methanol, 60 mol% for ethanol, and 50 mol% for both PA and IPA. Very similar results were obtained by Lam et al. with X-ray absorption spectroscopy showing weaker liquid–liquid interactions at IPA concentrations higher than 50 mol%.[25] The mesoscopic structure of aqueous IPA solutions was also studied by pressure perturbation calorimetry combined with molecular dynamics simulations which revealed segregation of water and alcohol molecules.[26] More rigorous molecular computations were recently performed to analyze the hydrogen bonding interactions in the IPA–water system, and strong microscopic inhomogeneities were identified.[27] It was shown that IPA molecules tend to be involved into water networks at low alcohol content, whereas water and IPA form segregated domains when the molar fraction of the alcohol increases from 0.3 to 0.5. In concentrated solutions, water molecules were found to interact with IPA molecules as separate solutes. Thus, the loss of the percolating water is likely to be responsible for the permeation slowdown observed with the alcohol-rich azeotrope.

In order to examine in detail the transition from a water-dominant phase to a more alcohol-like one, we noticed an interesting feature of the IPA–water VLE. From the shape of the respective *p-x-y* diagrams, it appears that at room temperature, the composition of the liquid and vapor phases is very similar for IPA molar fractions beyond 0.5.[28] On *x-y* diagrams, this observation translates to curves that are lying close to the straight $y = x$ line.[29] Accordingly, we undertook a simple experiment on measuring the vapor pressure in D_2O-IPA mixtures as a function of the total composition (**Figure 3**). As detailed earlier, this test allows to determine the azeotropic composition at a pressure extremum.[19] It is evident that room-temperature mixtures do reveal no clear minimum boiling point, and instead, there is a plateau-like region at high alcohol content. We assume that the molar composition of the vapor phase in this range can be approximated by the partial values as defined during the mixtures preparation. In the following, we show the transmembrane flux of water as measured upon gradual variation of the feed composition and rationalize the observed trend by devising a geometrical model to account for the structural rearrangements in the binary mixture.

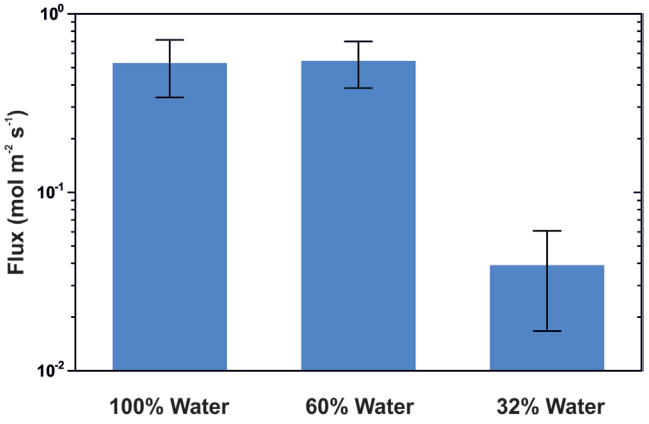

Figure 2. Transmembrane flux of D_2O molecules upon exposing CNMs to pure water vapor and its azeotropic mixtures with alcohols (60 mol% water in PA and 32 mol% water in IPA). The experimental data were averaged over 3–5 samples, and the error bars are standard deviations.

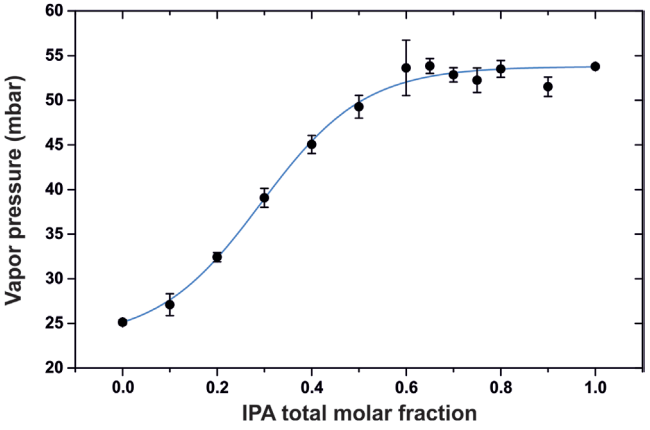

Figure 3. Saturation vapor pressure in D_2O-IPA mixtures as a function of the total composition. The experiment is detailed elsewhere.[19] The measurements were done at room temperature, and the data points are mean values over 3–6 runs. The solid line is for guiding the eye.

2.3. Kinetic Model

The rapid permeation of water vapor in CNMs was recently elucidated in terms of surface condensation and single-file diffusion.[20] The formalism implemented refers to adsorption isotherms and heterogeneous reaction kinetics as proposed in computational studies.[30] More specifically, the transmembrane flux of water molecules F is described by two rate constants k_{mono} and k_{multi} for individual and cooperative passage, respectively

$$F = k_{mono}\,\theta_{mono} n_0 + k_{multi}\theta_{multi} n_0 \quad (1)$$

where θ_{mono} and θ_{multi} designate surface coverage of separate adsorbates and their agglomerates, and n_0 stands for the total number of adsorption sites per unit area. The equation was proven to capture the steep humidity dependence and can also be used to simulate the permeation rate in mixtures with alcohols. As the ACP experiments with the model azeotropic mixtures are conducted under saturation conditions, similar to pure water, the membrane is likely to be fully covered with a condensed multilayer film (**Figure 4**). In this case, both water and alcohol molecules access the membrane proximity, and the amount of water in the first adsorption layer can be expressed via effective coverage θ_{eff}. It is clear that θ_{eff} should depend on the molar fraction x and span from 0 for anhydrous alcohol up to 1 for water-dominant solutions. More precisely, the coverage is proportional to the number concentration c as the number of molecules at the surface is nothing else than a number of molecules in a very thin volume. To derive the concentration as a function of x, we consider van der Waals volumes of molecules and neglect intermolecular voids. For simplicity, PA and IPA molecules are both assumed to be rods with the diameter of 0.29 nm.[31] In this representation, water molecules appear to be roughly three times as small as the alcohol ones,[19] and their concentration is expressed as follows

$$c = \frac{x}{(3-2x)\,v} \quad (2)$$

where v is the volume occupied by one D_2O molecule (unit volume in the model). On the basis of the experiments with PA (Figure 2) and in accordance with the above reviewed literature data, we set the boundary condition $\theta_{eff} = 1$ at $x \geq 0.6$ which yields the linear equation

$$\theta_{eff} = \frac{3x}{3-2x} \quad (3)$$

The next step is to understand how the rate constant for crossing the membrane is affected by mixing with alcohols. As dilution affects not only the number of water molecules, but also their dynamic behavior, Equation (1) transforms to

$$F = k_{eff}\,\theta_{eff} n_0 \quad (4)$$

where k_{eff} accounts for the transition from cooperative to individual motion. Clearly, the effective rate constant is also a function of the molar fraction, and the following boundary conditions apply

$$k_{eff} \to k_{mono}, \theta_{eff} \to 0 \quad (5)$$

$$k_{eff} \to k_{multi}, \theta_{eff} \to 1 \quad (6)$$

To obtain an analytical form for $k_{eff} = f(x)$, one can deepen the analogy between permeation through nanopores and chemical reactions by appealing to molecularity. If the single-file transport requires many molecules to be involved, it is reasonable to represent the rate constant as a power law of the molar fraction

$$k_{eff} = (k_{multi} - k_{mono})\left(\frac{x}{x_0}\right)^m + k_{mono} \quad (7)$$

where x_0 is the above critical molar fraction, and m is the kinetic order of the transmembrane passage. Under these circumstances, Equation (7) meets all the boundary conditions, and it can be plugged along with Equation (3) into Equation (4) to simulate water flux. As k_{mono} and k_{multi} were determined in the previous experiments,[20] the only model parameter is the order m whose physical meaning consists in the number of molecules taking part in a permeation event. **Figure 5** shows the results of

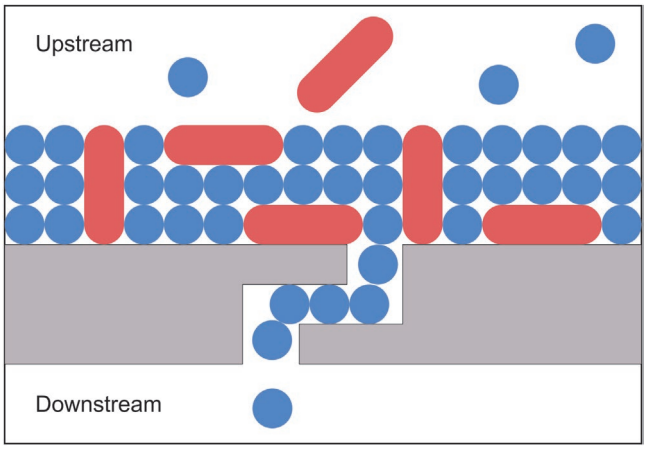

Figure 4. Adsorption model for kinetic simulations of water permeation in nanomembranes. Blue balls are for water molecules, red rods are for propanol molecules.

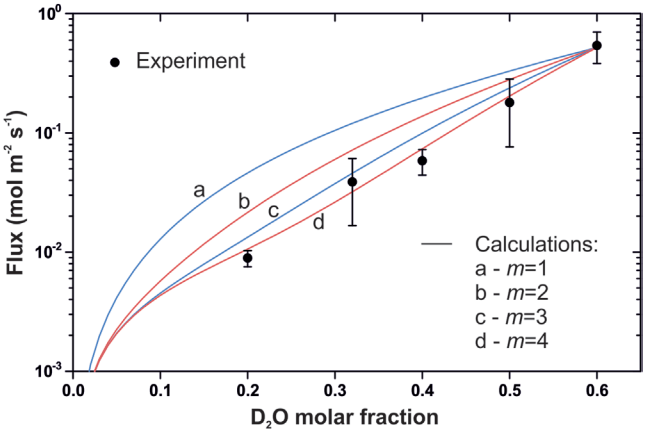

Figure 5. Experimental and theoretical flux of D_2O molecules in mixtures with propanol as a function of the molar fraction. The data points are mean values over 3–4 measurements. The calculations were performed with $k_{mono} = 2.0 \times 10^3\ s^{-1}$; $k_{multi} = 2.6 \times 10^4\ s^{-1}$; and $n_0 = 2.0 \times 10^{-5}$ mol m^{-2}.

the ACP measurements with IPA–water system at various x as well as the calculated curves for different values of m.

The mixtures of D_2O with IPA do appear to be suitable for adjusting the composition of the condensed phase, and the flux measured goes further down as the alcohol molar fraction increases. There is a pronounced nonlinear transition whereas the difference between 40% and 80% solutions comprises almost two orders of magnitude. It is noteworthy that the kinetic model reproduces the observed behavior quite well at $m > 3$. The agreement reflects that our simple notion on the role of 3D networks in collective transport is correct, and the single file does need multiple species to take part. The results also shed light on the mechanism of concentration polarization in pervaporation and vapor permeation processes because separation leads to the change of the molar composition at the membrane exterior. The recently discovered "molecular jamming" effect is essentially of the same origin as steric reasons cause the growth of alcohol concentration inside narrow nanochannels.[19] In that sense, a combination of water- and organic-selective membranes might be reasonable for different stages of the solvents recovery.

Figure 6 is the final demonstration of the phenomenon under investigation which consists in a nonstationary ACP measurement. Namely, it illustrates in real time how water flux sinks upon mixing with IPA. In this experiment, a portion of IPA was preliminary stored in the coldfinger, and then the feed compartment was saturated with D_2O vapor. As shown in the graph, the QMS signal was initially reaching a stable value while the pressure in the chamber was constant. Afterward, IPA was released from the small-volume coldfinger, and the pressure quickly rose up to around 50 mbar. Simultaneously, water vapor experienced a hydraulic shock as evidenced by a sharp spike in the transmembrane flux. This means water was forced to liquefy on the chamber walls and the membrane, so as its partial pressure dropped. What happened next was intermixing of the two substances and restoration of the saturated vapor. The total pressure in the system was monitored to slowly grow due to both evaporation of the compressed water and temperature fluctuations. However, the number of permeating molecules was found to decline steadily until the mixture was pumped away. Our interpretation of the effect observed is that the IPA molecules equilibrated with water not only in the gas phase, but also penetrated into the adsorbed layer. The alcohol was gradually diffusing through condensed water and thereby diminishing its concentration. Please note that the amount of IPA collected in the coldfinger was insufficient to create a liquid solution inside the vessel, and therefore, desorption of water from the membrane surface and its redistribution over the upstream chamber are excluded. Conversely, the addition of IPA would induce further condensation of water vapor as its partial pressure should be reduced in accordance with the VLE.

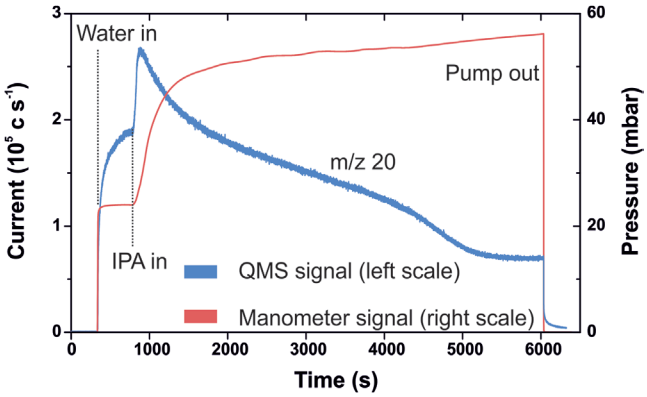

Figure 6. Transient ACP experiment with D_2O and IPA mixed during the measurement. The feed compartment was first saturated with D_2O vapor, and then IPA was let in. The QMS output for water molecules is aligned with the total pressure recording.

3. Conclusion

The ACP methodology was applied to investigate the transport of water molecules in model microporous membranes upon mixing with propanol. At room temperature, the flow rate was found to drop by orders of magnitude as the molar fraction of the alcohol increased from 0.4 to 0.8. The findings disclosed disruption of the single-file flow as a result of the structural changes in hydrogen bonding networks. The phenomenological model was proposed to explain the intermolecular rearrangements, and the kinetic simulations matched well the experimental data. Our study confirms previous theoretical predictions and reveals that the less water in the solution, the much slower its permeation. This observation may have implications for the engineering of membrane processes in separation of water–organic mixtures. Thus, the results obtained foresee challenges in applying nanostructured materials to dehydration of solvents. On the other hand, water-selective membranes can be effectively used to concentrate bioalcohols, although alcohol-selective membranes might be more practical at the final stages of upgrading.

4. Experimental Section

The ACP measurements were carried out at room temperature in a custom-made permeation setup with a mass spectrometer as detailed previously.[20] The nanomembrane windows used were ordinary CNMs suspended over S_3N_4/Si chips with 7 µm apertures. Terphenylthiol (Sigma-Aldrich, 97%) and Au(111) substrates (Georg Albert PVD) were used to prepare self-assembled monolayers followed by electron-induced conversion to CNMs.[22] Prior to experiments, D_2O (Sigma-Aldrich, 99.9% atom D) and isopropanol (Fisher Chemical, ≥99.8%) were degassed and stored in vacuum-sealed containers.

Acknowledgements

P.D. thanks the "Fonds der Chemischen Industrie" for a Liebig Fellowship and the "Max-Buchner-Forschungsstiftung" for a Max-Buchner Fellowship. M.R. thanks the German Academic Exchange Service (DAAD) for a Research Fellowship (Grant No. 57440917). The authors acknowledge the support from the German Federal Ministry for Education and Research (BMBF) (Grant Nos. 03XP0155A and 02WIL1453B).

Conflict of Interest

The authors declare no conflict of interest.

Keywords

adsorption controlled permeation, azeotrope separation, nanochannels, single-file water

Received: January 23, 2020
Revised: March 13, 2020
Published online: April 19, 2020

[1] a) C. Li, S. M. Meckler, Z. P. Smith, J. E. Bachman, L. Maserati, J. R. Long, B. A. Helms, *Adv. Mater.* **2018**, *30*, 1704953; b) Y. Peng, W. Yang, *Adv. Mater. Interfaces* **2020**, *7*, 1901514.

[2] a) Z. Cao, S. Zeng, Z. Xu, A. Arvanitis, S. Yang, X. Gu, J. Dong, *Sci. Adv.* **2018**, *4*, eaau8634; b) D. Kim, M. Y. Jeon, B. L. Stottrup, M. Tsapatsis, *Angew. Chem., Int. Ed.* **2018**, *57*, 480; c) Y. Li, H. Cao, J. Yu, *ACS Nano* **2018**, *12*, 4096.

[3] a) J. Sánchez-Laínez, L. Paseta, M. Navarro, B. Zornoza, C. Téllez, J. Coronas, *Adv. Mater. Interfaces* **2018**, *5*, 1800647; b) J. Hou, H. Zhang, G. P. Simon, H. Wang, *Adv. Mater.* **2019**, 1902009; c) W. Yang, Y. Zhu, Z. Sun, C. Gao, L. Xue, *Adv. Mater. Interfaces* **2019**, *6*, 1901482.

[4] a) N. Bui, E. R. Meshot, S. Kim, J. Peña, P. W. Gibson, K. J. Wu, F. Fornasiero, *Adv. Mater.* **2016**, *28*, 5871; b) J. K. Holt, H. G. Park, Y. Wang, M. Stadermann, A. B. Artyukhin, C. P. Grigoropoulos, A. Noy, O. Bakajin, *Science* **2006**, *312*, 1034; c) P. R. Kidambi, D. Jang, J.-C. Idrobo, M. S. H. Boutilier, L. Wang, J. Kong, R. Karnik, *Adv. Mater.* **2017**, *29*, 1700277.

[5] a) B.-Y. Guo, S.-D. Jiang, M.-J. Tang, K. Li, S. Sun, P.-Y. Chen, S. Zhang, *J. Phys. Chem. Lett.* **2019**, *10*, 4609; b) J. Shen, G. Liu, Y. Ji, Q. Liu, L. Cheng, K. Guan, M. Zhang, G. Liu, J. Xiong, J. Yang, W. Jin, *Adv. Funct. Mater.* **2018**, *28*, 1801511; c) K. Wang, I. R. Ausri, K. A. Chu, A. Seddon, X. Tang, *Adv. Mater. Interfaces* **2019**, *6*, 1802056.

[6] a) M. Fathizadeh, W. L. Xu, F. Zhou, Y. Yoon, M. Yu, *Adv. Mater. Interfaces* **2017**, *4*, 1600918; b) C. Chi, X. Wang, Y. Peng, Y. Qian, Z. Hu, J. Dong, D. Zhao, *Chem. Mater.* **2016**, *28*, 2921; c) H. Li, Z. Song, X. Zhang, Y. Huang, S. Li, Y. Mao, H. J. Ploehn, Y. Bao, M. Yu, *Science* **2013**, *342*, 95.

[7] a) X. Wang, Y. Zhao, E. Tian, J. Li, Y. Ren, *Adv. Mater. Interfaces* **2018**, *5*, 1701427; b) A. Akbari, P. Sheath, S. T. Martin, D. B. Shinde, M. Shaibani, P. C. Banerjee, R. Tkacz, D. Bhattacharyya, M. Majumder, *Nat. Commun.* **2016**, *7*, 10891; c) T. Van Gestel, J. Barthel, *J. Membr. Sci.* **2018**, *554*, 378.

[8] R. R. Nair, H. A. Wu, P. N. Jayaram, I. V. Grigorieva, A. K. Geim, *Science* **2012**, *335*, 442.

[9] a) M. Majumder, N. Chopra, R. Andrews, B. J. Hinds, *Nature* **2005**, *438*, 44; b) J. Hassan, G. Diamantopoulos, L. Gkoura, M. Karagianni, S. Alhassan, S. V. Kumar, M. S. Katsiotis, T. Karagiannis, M. Fardis, N. Panopoulos, H. J. Kim, M. Beazi-Katsioti, G. Papavassiliou, *J. Phys. Chem. C* **2018**, *122*, 10600; c) R. H. Tunuguntla, R. Y. Henley, Y.-C. Yao, T. A. Pham, M. Wanunu, A. Noy, *Science* **2017**, *357*, 792.

[10] K. S. Andrikopoulos, G. Bounos, D. Tasis, L. Sygellou, V. Drakopoulos, G. A. Voyiatzis, *Adv. Mater. Interfaces* **2014**, *1*, 1400250.

[11] R. K. Joshi, P. Carbone, F. C. Wang, V. G. Kravets, Y. Su, I. V. Grigorieva, H. A. Wu, A. K. Geim, R. R. Nair, *Science* **2014**, *343*, 752.

[12] a) J. Abraham, K. S. Vasu, C. D. Williams, K. Gopinadhan, Y. Su, C. T. Cherian, J. Dix, E. Prestat, S. J. Haigh, I. V. Grigorieva, P. Carbone, A. K. Geim, R. R. Nair, *Nat. Nanotechnol.* **2017**, *12*, 546; b) L. Chen, G. Shi, J. Shen, B. Peng, B. Zhang, Y. Wang, F. Bian, J. Wang, D. Li, Z. Qian, G. Xu, G. Liu, J. Zeng, L. Zhang, Y. Yang, G. Zhou, M. Wu, W. Jin, J. Li, H. Fang, *Nature* **2017**, *550*, 380.

[13] Y. Shin, M. F. N. Taufique, R. Devanathan, E. C. Cutsforth, J. Lee, W. Liu, L. S. Fifield, D. W. Gotthold, *Sci. Rep.* **2019**, *9*, 2251.

[14] L. M. Vane, *J. Chem. Technol. Biotechnol.* **2019**, *94*, 343.

[15] a) L. M. Vane, *Biofuels, Bioprod. Bioref.* **2008**, *2*, 553; b) Y. Huang, R. W. Baker, L. M. Vane, *Ind. Eng. Chem. Res.* **2010**, *49*, 3760; c) Y. Huang, J. Ly, D. Nguyen, R. W. Baker, *Ind. Eng. Chem. Res.* **2010**, *49*, 12067.

[16] Y. K. Ong, G. M. Shi, N. L. Le, Y. P. Tang, J. Zuo, S. P. Nunes, T.-S. Chung, *Prog. Polym. Sci.* **2016**, *57*, 1.

[17] A. Ghoufi, F. Artzner, P. Malfreyt, *J. Phys. Chem. B* **2016**, *120*, 793.

[18] D. Naberezhnyi, A. Gölzhäuser, P. Dementyev, *J. Phys. Chem. Lett.* **2019**, *10*, 5598.

[19] P. Dementyev, Y. Yang, M. Rezvova, A. Gölzhäuser, *J. Phys. Chem. Lett.* **2020**, *11*, 238.

[20] P. Dementyev, T. Wilke, D. Naberezhnyi, D. Emmrich, A. Gölzhäuser, *Phys. Chem. Chem. Phys.* **2019**, *21*, 15471.

[21] a) R. A. Dawe, D. M. T. Newsham, S. B. Ng, *J. Chem. Eng. Data* **1973**, *18*, 44; b) E. B. Munday, J. C. Mullins, D. D. Edie, *J. Chem. Eng. Data* **1980**, *25*, 191; c) C. Gabaldón, P. Marzal, J. B. Montón, M. A. Rodrigo, *J. Chem. Eng. Data* **1996**, *41*, 1176.

[22] a) Y. Yang, P. Dementyev, N. Biere, D. Emmrich, P. Stohmann, R. Korzetz, X. Zhang, A. Beyer, S. Koch, D. Anselmetti, A. Gölzhäuser, *ACS Nano* **2018**, *12*, 4695; b) Y. Yang, R. Hillmann, Y. Qi, R. Korzetz, N. Biere, D. Emmrich, M. Westphal, B. Büker, A. Hütten, A. Beyer, D. Anselmetti, A. Gölzhäuser, *Adv. Mater.* **2020**, *32*, 1907850.

[23] W. M. Langdon, D. B. Keyes, *Ind. Eng. Chem.* **1942**, *34*, 938.

[24] R. Li, C. D'Agostino, J. McGregor, M. D. Mantle, J. A. Zeitler, L. F. Gladden, *J. Phys. Chem. B* **2014**, *118*, 10156.

[25] R. K. Lam, J. W. Smith, R. J. Saykally, *J. Chem. Phys.* **2016**, *144*, 191103.

[26] J. W. Bye, C. L. Freeman, J. D. Howard, G. Herz, J. McGregor, R. J. Falconer, *J. Solution Chem.* **2017**, *46*, 175.

[27] Y. M. Muñoz-Muñoz, G. Guevara-Carrion, J. Vrabec, *J. Phys. Chem. B* **2018**, *122*, 8718.

[28] D. I. Shishin, A. L. Voskov, I. A. Uspenskaya, *Russ. J. Phys. Chem. A* **2010**, *84*, 1667.

[29] P. Marzal, J. B. Montón, M. A. Rodrigo, *J. Chem. Eng. Data* **1996**, *41*, 608.

[30] a) J. Schrier, *ACS Appl. Mater. Interfaces* **2012**, *4*, 3745; b) L. W. Drahushuk, M. S. Strano, *Langmuir* **2012**, *28*, 16671; c) C. Sun, M. S. H. Boutilier, H. Au, P. Poesio, B. Bai, R. Karnik, N. G. Hadjiconstantinou, *Langmuir* **2014**, *30*, 675.

[31] Y. Markus, *J. Phys. Org. Chem.* **2003**, *16*, 398.